A Meshfree Thin Shell for Arbitrary Evolving Cracks Based on An Extrinsic Basis

Timon Rabczuk[1] **and Pedro Areias**[2]

Abstract: This paper proposes a meshfree method for arbitrary evolving cracks in thin shells. The approach is an improvement of the method proposed by Rabczuk T., Areias P.M.A., Belytschko T. (A meshfree thin shell for large deformation, finite strain and arbitrary evolving cracks, International Journal for Numerical Methods in Engineering). In the above cited paper, a shell was developed based on an intrinsic basis of third order completeness. Third order completeness was necessary to remove membrane locking. This resulted in the use of very large domains of influence that made the method computationally expensive. If the crack was modelled by a set of cracked particles where the crack is introduced through the entire domain of influence, a very fine resolution was needed to capture the crack path. We will modify the method and use an extrinsic basis to increase the order of completeness of the approximation. The advantage is the saving in computational cost due to smaller domain of influences and coarser resolutions to capture the crack path. The method is applied to several crack problems and shows good agreement with experimental results.

keyword: Meshfree methods, Cracks, Cohesive models, KL constraint, Shell, Extrinsic basis.

1   Introduction

Thin shells have been studied with finite elements for many decades. Shells based on the satisfaction of the Kirchhoff-Love (KL) constraints require higher order elements and their development and implementation is very complex.

The discrete-Kirchhoff (non-conforming) finite elements deal with this constraint at a specified number of points and allow low order interpolation to be used (e.g. Herrmann (1967); Batoz, Hammadi, Zheng, and Zhong (2000)). Of particular interest here is the configuration with mid-side rotations (e.g. Fraeijs de Veubeke (1968);

Dawe (1972)). The semiloof element of Irons (1976) is a member of that family, but employs many nodes. The idea of using a *quadrilateral plate* with this configuration originates in the work of Fraeijs de Veubeke (1968) (Herrmann (1967) proposed the use of "crossed-triangles" to form a quadrilateral). It was later extended by Nagtegaal and Slater (1981), Batoz, Hammadi, Zheng, and Zhong (2000) and Crisfield and Tan (2001a).

Most work in *shell elements* with mid-side rotations employed either triangles Herrmann (1967); Dawe (1972); Peng, Merriman, and Osher (1999); Kolahi and Crisfield (2001) or *planar* quadrilaterals Batoz, Hammadi, Zheng, and Zhong (2000); Batoz, Zheng, and Hammadi (2001), often under very restrictive assumptions (e.g. Crisfield and Tan (2001a)) such as moderate rotations and co-rotational formulations based on the superposition of a plane element with a plate bending element, an assumption which is valid for triangular elements only. Non-symmetric shape functions are employed in references Nagtegaal and Slater (1981); Crisfield and Tan (2001b). A shell for finite rotations and finite strains was proposed by Atluri (1984); Atluri and Cazzani (1994).

Continuum based shells are usually simpler. They are developed based on a continuum element formulation by imposing structural assumptions, see Belytschko, Liu, and Moran (2000). Another advantage of continuum based shells is that it is straight forward to use continuum constitutive models.

Areias, Song, and Belytschko (2005) developed a new shell element that is a combination of the continuum based shell and classical shell theory. They adopt the kinematic assumptions and the convenience of the decoupled energy from the classical shell theory. From the continuum description, they made use of the generality provided by the strain energy, so that constitutive models developed for continua are easily applicable to shells. They also made use of mid-side rotations when they extended their methodology for crack propagation, (see Areias, Song, and Belytschko (????)).

In the meshfree context, three dimensional modelling of

---
[1] Institute for Numerical Mechanics, Technical University of Munich, Boltzmannstr. 15, D-85748 Garching b. Munich, Germany.

[2] Northwestern University, Department of Mechanical Engineering

shells and degenerated shells was carried out by Noguchi, Kawashima, and Miyamura (2000); Li, Hao, and Liu (2000); Kim, Choi, Chen, and Botkin (2002). D.D. and Chen (2004); Chen, Wang, and Dong (2004); Garcia, Fancello, de Barcellos, and Duarte (2000) studied plates and beams. Li, Soric, Jarak, and Atluri (2005) recently developed a locking-free thin and thick plate within the framework of the Meshless local Petrov Galerkin (MLPG) method, Atluri and Shen (2002); Atluri and Zhu (1998, 2000). Their results were compared to analytical solutions and showed excellent agreement. The main difference of the MLPG method to method such as the elementfree Galerkin (EFG) or Reproducing Kernel Particle Method (RKPM) is that local weak forms are generated on overlapping subdomains rather than using global weak forms. The integration of the weak form is then carried out in these local subdomains. Thus, the method is truly meshfree since no construction of a background mesh is needed for integration purposes, Atluri (2002). The first meshfree thin shell based on the imposition of the KL constraints was proposed by Krysl and Belytschko (1996). It was developed for small deformations, small strains and elasticity. Up to now, there are only a few research done on the incorporation of discontinuities in shells. Rabczuk, Areias, and Belytschko (submitted) developed a meshfree thin shell for large deformations, finite strains, nonlinear materials and cracks. Two different approaches to introduce the cracks were proposed. To remove membrane locking, the polynomial basis was third order complete. This led to very large domains of influence and high computational cost and memory problems for large problems when the shape functions are stored, even on parallel machines (up to 60 processors).

Within this paper, we pursue the idea in Rabczuk, Areias, and Belytschko (submitted) but use an extrinsic basis to remove membrane locking. Shepard functions are used that are easily computed and require very small domains of influence. Due to the smaller compact support, all shape functions can be stored; no or at least only a few data has to be taken from the main memory during the course of the computation.

The paper is arranged as follows: First, the meshfree method is explained. Then, the kinematics of the shell is described and the concept how to incorporate continuum constitutive models is reviewed in section 5. The cohesive crack model is explained afterwards. Finally, we ap-

ply the method to some cracking problems and compare the results to experimental data.

2   Meshfree Method

In meshfree methods, there are different ways to increase the order of completeness. In the element-free Galerkin method, see e.g. Belytschko, Lu, and Gu (1994); Belytschko and Lu (1995), the order of completeness is determined intrisically by the polynomial basis $\mathbf{p}$ while in the $h - p$-cloud method (Duarte and Oden (1996a,b)) or in the partition of unity finite element method (PUFEM), Melenk and Babuska (1996), the order of completeness is determined by an extrinsic basis. The advantage of an extrinsic basis is that the shape functions are simpler and simpler to compute but therefore additional degrees of freedom are introduced. For thin shells, at least quadratic polynomial basis is required. However, a quadratic basis can lead to membrane locking that can be eliminated by third order completeness. We therefore use cubic polynomial basis $\mathbf{p}$ but instead of using an intrinsic basis as in Rabczuk, Areias, and Belytschko (submitted), we will use an extrinsic basis:

$$u^h(\mathbf{X},t) = \sum_{J \in S} \Phi_J(\mathbf{X}) \left(u_J(t) + \sum_{I=1}^{N} \mathbf{p}_I(\mathbf{X}) \, \mathbf{a}_{JI} \right) \qquad (1)$$

where $\Phi_J(\mathbf{X})$ are the shape functions, $\mathbf{p}$ is the third order polynomial basis, $\mathbf{u}$ and $\mathbf{a}$ are nodal parameters, S is the set of nodes where $\Phi_J(\mathbf{X}) \neq 0$ and N is the number of the polynomial basis. The Shepard function $\Phi_J(\mathbf{X})$ fulfills zero-order completeness and is given by:

$$\Phi_J(\mathbf{X}) = \frac{w_J(\mathbf{X},h)}{\sum\limits_{J \in S} w_J(\mathbf{X},h)} \qquad (2)$$

Here, $w_J(\mathbf{X},h)$ is the weight function, also called kernel function and h determines the size of the domain of influence of the weight function. We have chosen quartic spline that is C^2 continuous. For the Shepard function, there are no requirements with respect to the number of neighboring particles as in higher order MLS shape functions where a minimum number of neighboring particles are needed (depending on the degree of completeness). The derivatives of the Shepard functions are also simple to compute. One drawback of an extrinsic basis is that it leads to ill-conditioning of the stiffness matrix, Duarte and Oden (1996a,b). The conditioning of the matrix can be improved by a Gram-Schmidt orthogonalization.
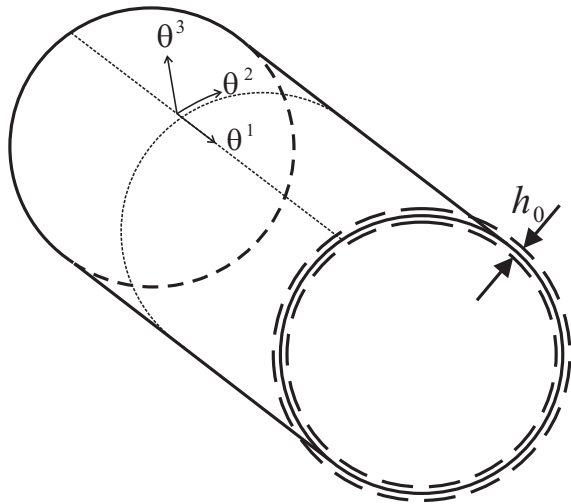
Figure 1 : Surface parametrization for a cylinder

Note that, in the following sections curvilinear coordinates will be used as they are particularly convenient in the interpenetration of the momentum equation.

3 Shell Model

Consider a material point $\mathbf{X} \in \Omega_0$ of the shell in the reference configuration that is described by

$$\mathbf{X}(\theta^i) = \mathbf{R}(\theta^\alpha) + \theta^3 \, \mathbf{N}(\theta^\alpha) \tag{3}$$

where θ^i with $i = 1, 2, 3$ are curvilinear coordinates, $\mathbf{N}$ is the shell normal and $\mathbf{R}$ is a point on the shell surface in the reference configuration $\mathcal{S}_0$. Upper Latin and Greek indices are ranging from 1 to 3 and from 1 to 2, respectively where the coordinate θ^3 represents the signed distance to the reference surface. The most difficult part is the surface parametrization. We use Lagrangian coordinates to parametrize the shell's midplane. Different parametrization are used for different shapes. For a cylindrical shell, the vector from the origin of a spatially fixed coordinate system to the undeformed midplane $\mathbf{R}$ is given by (see also figure 1)

$$\mathbf{R} = \left(\sin\theta^2, \cos\theta^2, \theta^1 \right) \tag{4}$$

For rectangular shells, the surface parametrization is straightforward. More complicated geometries can be generated by assembling some basic geometries. For example, a complicated honeycomb sandwich structure can be considered as composition of many rectangular shells.

These shells can be connected by Lagrange multipliers at their interfaces.

The first and second fundamental forms are given by

$$A_{\alpha\beta} = \mathbf{R}_{,\alpha} \cdot \mathbf{R}_{,\beta} \tag{5}$$

$$B_{\alpha\beta} = \mathbf{R}_{,\alpha,\beta} \cdot \mathbf{N} = -\mathbf{R}_{,\alpha} \cdot \mathbf{N}_{,\beta} \tag{6}$$

The curvilinear coordinates θ^α are such that $\mathbf{R}_{,\alpha}$ form a basis for the tangent space in $X \in \mathcal{S}_0$. For arbitrary θ^3, we define a family of surfaces $\mathcal{S}_0(\theta^3)$ with $\mathcal{S}_0(0) = \mathcal{S}_0$ for which the tangent basis is established from eq. (3) as $\mathbf{X}_{,\alpha} = \mathbf{R}_{,\alpha} + \theta^3 \mathbf{N}_\alpha$. If we extend this basis by including $\mathbf{N} = \mathbf{X}_{,3}$, the resulting basis spans Ω_0, and we can then define the metric of Ω_0 as $G_{ij} = \mathbf{X}_{,i} \cdot \mathbf{X}_{,j}$. The dual basis is given by $\mathbf{G}^i = G^{ij}\mathbf{X}_{,j}$ with $\left[G^{ij} \right] = [G_{ij}]^{-1}$.

The Cauchy-Green tensor can be given as

$$\mathbf{C} = \mathbf{F}^T \mathbf{F} = \underbrace{(\mathbf{x}_{,i} \cdot \mathbf{x}_{,j})}_{C_{ij}} \mathbf{G}^i \otimes \mathbf{G}^j \tag{7}$$

The Kirchhoff-Love hypothesis states that $\mathbf{N}$ is perpendicular to $\mathbf{R}$:

$$\mathbf{N} = \frac{\mathbf{R}_{,\alpha} \times \mathbf{R}_{,\beta}}{\|\mathbf{R}_{,\alpha} \times \mathbf{R}_{,\beta}\|} \quad , \|\mathbf{N}\| = 1 \tag{8}$$

4 Discretization

4.1 Displacement field

The approximation of a point on the shell surface is given by

$$\mathbf{r}(\theta^\alpha, t) = \mathbf{r}^{\text{cont}}(\theta^\alpha, t) + \mathbf{r}^{\text{enr}}(\theta^\alpha, t) \tag{9}$$

where the first term on the RHS of eq. (9) is the continuous part and the second term on the RHS is the enrichment. Let $\mathcal{N}$ be the total set of nodes in the model and $\mathcal{N}_c$ the set of cracked nodes. To model the discontinuous part of the displacement, the test and trial functions are enriched with sign functions which are parametrized by $\delta\mathbf{q}_I$ and $\mathbf{q}_I$, respectively. The trial functions are

$$\mathbf{r}(\theta^\alpha, t) = \sum_{I \in \mathcal{N}} \Phi_I(\theta^\alpha) \left(\mathbf{r}_I(t) + \sum_{J=1}^{N} \mathbf{p}_J(\theta^\alpha)\mathbf{a}_{IJ} \right)$$

$$+ \sum_{I \in \mathcal{N}_c} \Phi_I(\theta^\alpha) \, S[f_I(\theta^\alpha)] \left(\mathbf{q}_I(t) + \sum_{J=1}^{N} \tilde{\mathbf{p}}_J(\theta^\alpha)\mathbf{b}_{IJ} \right) \tag{10}$$

The first line of the RHS of eq. (10) represents the continuous part. Hereby, **a** are additional unknowns that are introduced to increase the order of completeness as already mentioned in the introduction and in section 2. The second and third line of eq. (10) is the enrichment. Our first intention was to use the Shepard functions without further extrinsic basis, represented by the additional unknowns **b**. This resulted in unstable results and unrealistic crack paths. However, we found that the extrinsic basis for the enrichment $\tilde{\mathbf{p}}$ can be of lower order-second order completeness in our case- than the continuous extrinsic basis **a**. Alternatively, one could also use an intrinsic basis for the enrichment:

$$\mathbf{r}(\theta^\alpha, t) = \sum_{I \in \mathcal{N}} \Phi_I(\theta^\alpha) \left(\mathbf{r}_I(t) + \sum_{J=1}^{N} \mathbf{p}_J(\theta^\alpha)\mathbf{a}_{IJ} \right)$$
$$+ \sum_{I \in \mathcal{N}_c} \tilde{\Phi}_I(\theta^\alpha) \, S[f_I(\theta^\alpha)] \, \mathbf{q}_I(t) \tag{11}$$

where $\tilde{\Phi}$ are second order complete MLS shape functions. Strouboulis, Copps, and Babuška (2000) showed that it is admissible to use different order of shape functions for the continuous and discontinuous part. Accordingly, the test functions can be expressed:

$$\delta\mathbf{r}(\theta^\alpha, t) = \sum_{I \in \mathcal{N}} \Phi_I(\theta^\alpha) \left(\delta\mathbf{r}_I(t) + \sum_{J=1}^{N} \mathbf{p}_J(\theta^\alpha)\delta\mathbf{a}_{IJ} \right)$$
$$+ \sum_{I \in \mathcal{N}_c} \Phi_I(\theta^\alpha) \, S[f_I(\theta^\alpha)] \left(\delta\mathbf{q}_I(t) + \sum_{J=1}^{N} \tilde{\mathbf{p}}_J(\theta^\alpha)\delta\mathbf{b}_{IJ} \right) \tag{12}$$

or

$$\delta\mathbf{r}(\theta^\alpha, t) = \sum_{I \in \mathcal{N}} \Phi_I(\theta^\alpha) \left(\delta\mathbf{r}_I(t) + \sum_{J=1}^{N} \mathbf{p}_J(\theta^\alpha)\delta\mathbf{a}_{IJ} \right)$$
$$+ \sum_{I \in \mathcal{N}_c} \tilde{\Phi}_I(\theta^\alpha) \, S[f_I(\theta^\alpha)] \, \delta\mathbf{q}_I(t) \tag{13}$$

where $f_I(\theta^\alpha)$ is given by

$$f_I(\theta^\alpha) = \mathbf{m} \cdot (\theta^\alpha - \theta_I^\alpha) \tag{14}$$

where **m** is the normal to the crack and the sign function $S(\xi)$ is defined as:

$$S(\xi) = \begin{cases} 1 & \forall \xi > 0 \\ -1 & \forall \xi < 0 \end{cases} \tag{15}$$

Note, that particles across the crack are excluded from the usual domain of influence. Note also that nodal stresses are obtained by MLS fit.

The director field **n** can be obtained from eq. (8). For the variation of **x** (and their spatial derivatives) given by

$$\delta\mathbf{x} = \delta\mathbf{r} + \theta^3 \delta\mathbf{n} \tag{16}$$

the variation of the normal has to be computed, that can be expressed in terms of **r**

$$\delta\mathbf{n} = \frac{1}{\|\mathbf{r}_{,\alpha} \times \mathbf{r}_{,\beta}\|} \left(\mathbf{I} - \mathbf{n} \otimes \mathbf{n}\right) \left(\delta\mathbf{r}_{,\alpha} \times \mathbf{r}_{,\beta} + \mathbf{r}_{,\alpha} \times \delta\mathbf{r}_{,\beta}\right) \tag{17}$$

The jump in the displacement field is

$$[[\mathbf{x}]] = [[\mathbf{r}]] + \theta^3 [[\mathbf{n}]] \tag{18}$$

where the jump in the director is given via $[[\mathbf{r}]]$:

$$[[\mathbf{n}]] = \mathbf{n}^+ - \mathbf{n}^- = \frac{\mathbf{r}_{,\alpha}^+ \times \mathbf{r}_{,\beta}^+}{\|\mathbf{r}_{,\alpha}^+ \times \mathbf{r}_{,\beta}^+\|} - \frac{\mathbf{r}_{,\alpha}^- \times \mathbf{r}_{,\beta}^-}{\|\mathbf{r}_{,\alpha}^- \times \mathbf{r}_{,\beta}^-\|} \tag{19}$$

We finally note that in the absence of the crack, we have 12 nodal parameters to guarantee third order completeness. Note that we only use the Shepard function as shape function. For nodes that are influenced by a crack, additional 9 nodal parameters are used in case of an extrinsic enrichment using Shepard functions. Alternatively, we have added 3 additional nodal degrees of freedom and used second order complete MLS shape functions. This has the drawback that the domain of influence increases significantly. However, since only few nodes are influenced by the crack, this effect plays a minor role.

4.2 Momentum equation

The weak form of the momentum equation is written in the form of the principle of virtual work (see e.g. Belytschko, Liu, and Moran (2000)): find $\mathbf{u} \in \mathcal{V}$ such that

$$\delta W = \delta W_{int} - \delta W_{ext} + \delta W_{kin} = 0 \quad \forall \delta\mathbf{u} \in \mathcal{V}_0 \tag{20}$$

where

$$\mathcal{V} = \left\{ \mathbf{r}(\cdot, t) | \mathbf{r}(\cdot, t) \in H^2 \; \mathbf{r}(\cdot, t) = \bar{\mathbf{r}}(t) \right.$$
$$\left. on \; \Gamma_0^u, \; \mathbf{r}(\cdot, t) \text{ discontinuous on } \Gamma_0^c \right\}$$

$$\mathcal{V}_0 = \left\{ \delta\mathbf{r} | \delta\mathbf{r} \in \mathcal{V}, \; \delta\mathbf{r} = 0 \right.$$
$$\left. on \quad \Gamma_u, \; \delta\mathbf{r} \text{ discontinuous on } \Gamma_0^c \right\} \tag{21}$$

$$\delta W_{int} = \int_{\Omega_0} s^{\alpha\beta} \mathbf{x}_{,\alpha} \cdot \delta \mathbf{x}_{,\beta} \, \mathbf{G}_1 \cdot (\mathbf{G}_2 \times \mathbf{G}_3) d\Omega \qquad (22)$$

$$\delta W_{ext} = \int_{\Omega_0 \setminus \Gamma_0^c} \rho_0 \, \mathbf{b} \cdot \delta \mathbf{u} \, d\Omega_0 + \int_{\Gamma_0^t} \bar{\mathbf{t}}_0 \cdot \delta \mathbf{u} \, d\Gamma_0$$
$$+ \int_{\Gamma_0^c} \bar{\mathbf{t}}_0^c \cdot \delta[[\mathbf{u}]] \, d\Gamma_0 \qquad (23)$$

$$\delta W_{kin} = \int_{\Omega_0} \rho_0 \, \delta \mathbf{u} \cdot \ddot{\mathbf{u}} \, d\Omega_0 \qquad (24)$$

where the prefix δ denotes the test function and W_{ext} is the external energy, W_{int} designates the internal energy and W_{kin} the kinetic energy. We use a background mesh to integrate the governing equations so that a background cell is created by four particles. To integrate the terms across the crack effectively, a sub-triangulation of the background cell is usually performed. This requires the introduction of sub-triangular integration cells. We will pursue another idea first proposed by Song, Areias, and Belytschko (2006) in the context of finite elements and modify the quadrature weights.

Therefore, the element area is subdivided into cells by a Voronoi procedure as shown in figure 2, simplified for the case of 9 Gauss points. This procedure is straightforward since a Delauny triangulation is already implemented in the code.

The sum of the area of the Voronoi cells A_i will be the area of the background cell A_{total} in the parent domain:

$$\sum_i A_i = A_{total} \qquad (25)$$

The quadrature weights of the Gauss points whose area is not crossed by the discontinuity are unmodified, otherwise the weights are computed by:

$$W_i^+ = W_i \frac{A_i^+}{A_i}$$
$$W_i^- = W_i \frac{A_i^-}{A_i} \qquad (26)$$

For more details, see Rabczuk, Areias, and Belytschko (submitted); Rabczuk and Belytschko (2004, 2006).

5 Constitutive Models

5.1 *Continuum model*

We used the contravariant components of the Kirchhoff stress tensor (which are identical to the components of
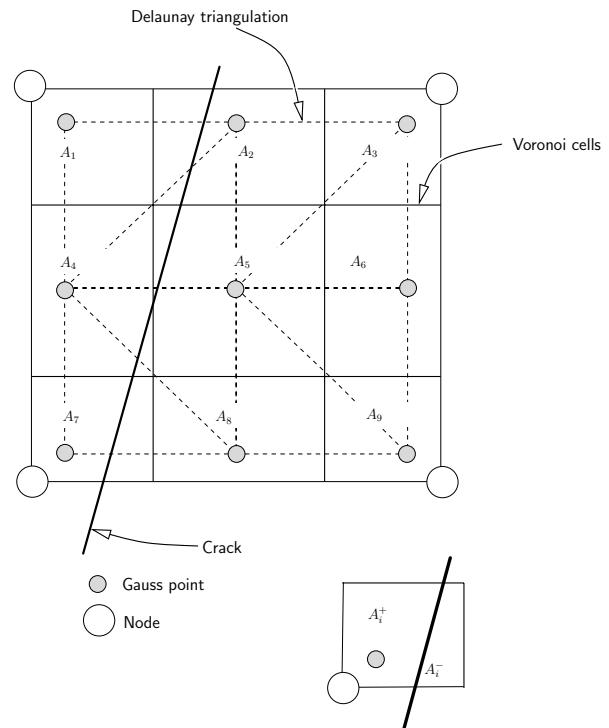

Figure 2 : Integration with background cells across the crack

the second Piola-Kirchhoff stress tensor in the material basis) to establish the weak form of equilibrium equations for the shell model. Our shell model corresponds to a 2D theory, yielding computational savings in non-linear inelastic analysis. To take advantage of the simplicity of our previous derivations, we retain the curvilinear coordinates in the inelastic range. We use a 2D model for the radial return and rotate so that the 3-3 component corresponds to the normal. For more details, see Rabczuk, Areias, and Belytschko (submitted).

We use the large strain elasto-plastic model introduced by Miehe (1998) with appropriate modifications and simplifications to adapt it to our shell model. For example, in contrast with Miehe, we do not use a spectral decomposition of the Cauchy-Green tensor and opt to use Padé interpolants. Note that this corresponds to the *dual* formulation of elasto-plasticity Han and Reddy (1999) (in stress space) and is now a classical procedure in many applications. For this reason, and because we limit ourselves to *isotropic* constitutive laws, we only present the main results. The formulation follows the multiplicative decomposition of the deformation gradient $\mathbf{F}$, proposed

by Lee (1969):

$$\boldsymbol{F} = \boldsymbol{F}^e \boldsymbol{F}^p \qquad (27)$$

and *define* the right Cauchy-Green tensors (elastic and plastic) accordingly:

$$\boldsymbol{C}^e = \boldsymbol{F}^{e^T} \boldsymbol{F}^e$$

$$\boldsymbol{C}^p = \boldsymbol{F}^{p^T} \boldsymbol{F}^p$$

With this notation, we can introduce a unsymmetric tensor $\boldsymbol{C}^E$ (we retain some nomenclature close to what was introduced in Miehe (1998)) such as:

$$\boldsymbol{C} = \boldsymbol{C}^E \boldsymbol{C}^p \qquad (28)$$

$\boldsymbol{C}^E$ can be written as a function of $\boldsymbol{C}^e$ according to:

$$\left(\boldsymbol{C}^E\right)^T = \boldsymbol{F}^{p^{-1}} \boldsymbol{C}^e \boldsymbol{F}^p \qquad (29)$$

The formulation does not rely on the actual identification of $\boldsymbol{F}^e$ or $\boldsymbol{F}^p$ and these quantities remain undetermined in the present work. Making use of a spectral decomposition of $\boldsymbol{C}^e$ and relating it to $\boldsymbol{C}^E$, we make further progress by identifying that they possess analogous forms:

$$\boldsymbol{C}^e = \boldsymbol{N} \boldsymbol{E} \boldsymbol{N}^T \qquad (30)$$

with $\boldsymbol{N}$ being a matrix containing, column-wise, the *unitary* eigenvectors of $\boldsymbol{C}^e$ and $\boldsymbol{E} = \mathrm{diag}[\lambda_i^2]$ where λ_i are the principal *elastic* stretches. Let us insert (30) into (29) to obtain:

$$\boldsymbol{C}^E = \left(\boldsymbol{F}^{p^T} \boldsymbol{N}\right) \boldsymbol{E} \left(\boldsymbol{F}^{p^T} \boldsymbol{N}\right)^{-1} \qquad (31)$$

If we introduce $\boldsymbol{N}^E = \boldsymbol{F}^{p^T} \boldsymbol{N}$ then it is clear that $\boldsymbol{C}^p$ can be expressed as:

$$\boldsymbol{C}^p = \boldsymbol{N}^E \boldsymbol{N}^{E^T} \qquad (32)$$

and a more concise decomposition of $\boldsymbol{C}^E$ is obtained, identifying $\boldsymbol{N}^E$ as the matrix of *right* eigenvectors of $\boldsymbol{C}^E$:

$$\boldsymbol{C}^E = \boldsymbol{N}^E \boldsymbol{E} \boldsymbol{N}^{E^{-1}} \qquad (33)$$

Using (33), we can write the spectral decomposition of $\boldsymbol{C}$, as a counterpart of (30), keeping in mind that $\boldsymbol{N}^E$ is not generally composed of unitary vectors (as is $\boldsymbol{N}$):

$$\boldsymbol{C} = \boldsymbol{N}^E \boldsymbol{E} \boldsymbol{N}^{E^T} \qquad (34)$$

These elementary derivations are, however, purposeless if $\boldsymbol{C}^p$ is obtained directly from $\boldsymbol{F}^p$. Let us introduce a isotropic strain energy density as a function of the state variables $\boldsymbol{C}$, which is a measure of total strain, $\boldsymbol{C}^p$ which is a measure of plastic strain, and $\boldsymbol{\xi}$ which represents the set of remaining internal variables of state. We use the usual notation ψ for the strain energy function:

$$\psi \equiv \psi(\boldsymbol{C}, \boldsymbol{C}^p, \boldsymbol{\xi}) \qquad (35)$$

The evolution laws of both $\boldsymbol{C}^p$ and $\boldsymbol{\xi}$ are derived as to comply, *ab-initio*, with the second law of thermodynamics, which can be written using the Clausius-Planck inequality, in the absence of thermal terms:

$$\mathcal{D}_{\mathrm{int}} = \frac{1}{2} \boldsymbol{S} : \dot{\boldsymbol{C}} - \dot{\psi} \geq 0 \qquad (36)$$

where $\mathcal{D}_{\mathrm{int}}$ is the so-called internal dissipation. Inserting the time-derivative of (35) into (36) it is possible to write:

$$\mathcal{D}_{\mathrm{int}} = \left(\frac{1}{2} \boldsymbol{S} - \frac{\partial \psi}{\partial \boldsymbol{C}}\right) : \dot{\boldsymbol{C}} - \boldsymbol{S}^p : \dot{\boldsymbol{C}}^p - \boldsymbol{\chi} : \dot{\boldsymbol{\xi}} \geq 0 \qquad (37)$$

where $\boldsymbol{S}^p = \frac{\partial \psi}{\partial \boldsymbol{C}^p}$ and $\boldsymbol{\chi} = \frac{\partial \psi}{\partial \boldsymbol{\xi}}$. Using the fact that, in the absence of plastic evolution and "frozen" internal variable evolution (i.e. $\dot{\boldsymbol{\xi}} = 0$) the constitutive law should still satisfy (37) and the acompaining process is said to be non-dissipative ($\mathcal{D}_{\mathrm{int}} = 0$), we should be able to write $\boldsymbol{S} = 2\frac{\partial \psi}{\partial \boldsymbol{C}}$ for this condition to hold for arbitrary $\dot{\boldsymbol{C}}$. Note that $\dot{\boldsymbol{C}}^p = 0$ does *not* generally imply that $\dot{\boldsymbol{\xi}} = 0$, but this is assumed to hold in this work. The evolution laws are obtained from a "potential" of dissipation, which is here denoted as:

$$\mathcal{F} \equiv \mathcal{F}(\boldsymbol{C}^p, \boldsymbol{\xi}; \boldsymbol{S}^p, \boldsymbol{\chi}) \qquad (38)$$

from which we postulate that:

$$\dot{\boldsymbol{C}}^p = \dot{\alpha} \frac{\partial \mathcal{F}}{\partial \boldsymbol{S}^p}$$

$$\dot{\boldsymbol{\xi}} = \dot{\alpha} \frac{\partial \mathcal{F}}{\partial \boldsymbol{\chi}}$$

where $\dot{\alpha} \geq 0$ is a plastic parameter.

Let us introduce the elastic part of the strain energy function (the strain energy function can be decomposed into elastic and plastic parts, e.g. Han and Reddy (1999)). as a function of the principal elastic stretches: $\psi^e \equiv \psi^e(\lambda_i)$ with $i = 1, 2, 3$. If we introduce the principal *elastic* Hencky strain components as $\varepsilon_i = \ln\lambda_i$, and the principal Kirchhoff stress components as $\tau_i = \frac{\partial \psi^e}{\partial \varepsilon_i}$, it is possible to express, under coaxiality conditions, the second Piola-Kirchhoff stress tensor as:

$$\boldsymbol{S} = \boldsymbol{N}^{E^{-T}} \boldsymbol{S}_D \boldsymbol{N}^{E^{-1}} = s^{\alpha\beta} \boldsymbol{X}_{,\alpha} \otimes \boldsymbol{X}_{,\beta} \tag{39}$$

with $\boldsymbol{S}_D = \mathrm{diag}\left[\frac{\tau_i}{\lambda_i^2}\right]$. A conjugate force to the plastic metric $\boldsymbol{C}^p$ is $\boldsymbol{S}^p$, the plastic force, which can be written as:

$$\boldsymbol{S}^p = \frac{\partial \psi^e}{\partial \boldsymbol{C}^p} = \frac{1}{2}\boldsymbol{C}^{p-1}\boldsymbol{C}\boldsymbol{S} \tag{40}$$

where use was made of the chain rule and symmetry of $\boldsymbol{C}^p$, $\boldsymbol{C}$ and $\boldsymbol{S}$ and the symmetry of the result:

$$\frac{\partial \psi}{\partial \boldsymbol{C}^p} = \frac{\partial \psi}{\partial \boldsymbol{C}} : \frac{\partial \boldsymbol{C}}{\partial \boldsymbol{C}^p} = \frac{1}{2}\boldsymbol{S}\boldsymbol{C}^E = \frac{1}{2}\boldsymbol{C}^{E^T}\boldsymbol{S} \tag{41}$$

The term $\boldsymbol{C}\boldsymbol{S}$ in (40) is the so-called mixed-variant stress tensor Maugin (1994); Miehe (1998); Areias, César de Sá, and António (2003), and is here denoted as $\boldsymbol{\Sigma}$. This tensor is generally unsymmetric.

Finally, the flow law can be written as:

$$\dot{\boldsymbol{C}}^p = 2\dot{\alpha}\frac{\partial \mathcal{F}}{\partial \boldsymbol{\Sigma}}\boldsymbol{C}^p \tag{42}$$

and the elastic law is given by:

$$\boldsymbol{\Sigma} = \kappa\mathrm{tr}\boldsymbol{\varepsilon}\boldsymbol{I} + \mu\mathrm{dev}\boldsymbol{\varepsilon} \tag{43}$$

with

$$2\boldsymbol{\varepsilon} = \ln\boldsymbol{C}^E$$

Let us now integrate the flow law (42) using the exponential mapping, by introducing two time steps t_n and t_{n+1} (a

Table 1 : The return mapping in the material setting; encapsulation of the small strain case

Make $\boldsymbol{C}_0^p = \boldsymbol{I}$ (and therefore $\boldsymbol{C}_0^{p-1} = \boldsymbol{I}$) and $\boldsymbol{\xi}_0 = \boldsymbol{0}$ for all quadrature points

For each quadrature point at time-step n, perform the following calculations

1) Using the current position field $\boldsymbol{x}$ calculate $\boldsymbol{C}_{n+1} = (\boldsymbol{x}_{,\alpha} \cdot \boldsymbol{x}_{,\beta})\boldsymbol{G}^\alpha \otimes \boldsymbol{G}^\beta$ with $\boldsymbol{G}^\alpha = G^{\alpha\beta}\boldsymbol{X}_{,\beta}$ and $[G^{\alpha\beta}] = [\boldsymbol{X}_{,\alpha} \cdot \boldsymbol{X}_{,\beta}]^{-1}$

2) Calculate the trial of the elastic measure $\boldsymbol{C}_{n\star}^E = \boldsymbol{C}_{n+1}\boldsymbol{C}_n^{p-1}$

3) Use a second order Padé approximation to calculate $\boldsymbol{\varepsilon}_{n\star} = \frac{1}{2}\ln\boldsymbol{C}_{n\star}^E$

4) Using a *modified* (unsymmetric) small strain return-mapping algorithm, update $\boldsymbol{\xi}_n$ and calculate $\boldsymbol{\varepsilon}_{n+1}$ $\Delta\alpha$, $\boldsymbol{\Sigma}$ and the small strain consistent modulus $\mathbf{C}$

5) Calculate the new plastic metric inverse as $\boldsymbol{C}_{n+1}^{p-1} = \boldsymbol{C}_{n+1}^{-1}\exp[2\boldsymbol{\varepsilon}_{n+1}]$ using a first order Padé approximation for the exponential function

6) Calculate the contravariant components of the stress as

$$s^{\alpha\beta} = \boldsymbol{G}^\alpha \cdot \left(\boldsymbol{C}^{-1}\boldsymbol{\Sigma}\boldsymbol{G}^\beta\right)$$

and the contravariant components of the tangent modulus as

$$C^{\alpha\beta\gamma\delta} = G^{\alpha i}G^{\beta j}G^{\gamma k}G^{\delta l}C_{ijkl}$$

with $G^{\alpha i} = \boldsymbol{G}^\alpha \cdot \boldsymbol{e}_i$ for any $i = 1, 2, 3$ and $\alpha = 1, 2$.

time increment denoted $\Delta t = t_{n+1} - t_n$) and the variation of the plastic multiplier between these two instants ($\Delta\alpha$):

$$\boldsymbol{C}_{n+1}^E = \boldsymbol{C}_{n\star}^E \exp\left[-2\Delta\alpha\frac{\partial \mathcal{F}}{\partial \boldsymbol{\Sigma}}\right] \tag{44}$$

where $\boldsymbol{C}_{n\star}^E$ is given by:

$$\boldsymbol{C}_{n\star}^E = \boldsymbol{C}_{n+1}\boldsymbol{C}_n^{p-1} \tag{45}$$

or, making use of the notation $\boldsymbol{\varepsilon}_{n+1}$ and $\boldsymbol{\varepsilon}_{n\star}$:

$$\boldsymbol{\varepsilon}_{n+1} = \boldsymbol{\varepsilon}_{n\star} - \Delta\alpha\frac{\partial \mathcal{F}}{\partial \boldsymbol{\Sigma}} \tag{46}$$

Note that the finite strain consistent modulus can be written, using the chain rule, as a function of a "small strain" modulus **C** using indicial notation:

$$C_{ijkl} = \frac{\partial S_{ij}}{\partial C_{kl}} = C_{ir}^{-1} \mathbf{C}_{rjpq} \frac{\partial \varepsilon_{pq}}{\partial C_{kv}^E} C_{lv}^{p^{-1}} - C_{ik}^{-1} C_{lr}^{-1} \Sigma_{rj} \quad (47)$$

With (47) we can write the classical relation between the second Piola-Kirchhoff stress and the Green-Lagrange strain $E_2 = \frac{1}{2}\mathbf{C} - \frac{1}{2}\mathbf{I}$ as $\dot{\mathbf{S}} = 2\mathbf{C} : \dot{\mathbf{E}}_2$.

The small strain analogy of (46) allows us to use a small strain elasto-plastic code, adequately modified to deal with unsymmetric stress and strain tensors. It is interesting to note that approximations to logarithms and exponentials can be employed, as these are found to be sufficient in metal plasticity, even for considerably large strains. The algorithm in table 1 shows the adopted procedure. We use first order approximations for the exponential and second order for the logarithm functions:

$$\varepsilon \cong \varepsilon^1 = \varepsilon^0 \left(\mathbf{I} - \frac{1}{3}\varepsilon^0\varepsilon^0 \right)^{-1} \quad (48a)$$

with

$$\varepsilon^0 = \left(\mathbf{C}^E - \mathbf{I} \right) \left(\mathbf{C}^E + \mathbf{I} \right)^{-1} \quad (48b)$$

and

$$\mathbf{C}^E \cong (\mathbf{I} - \varepsilon)^{-1} (\mathbf{I} + \varepsilon) \quad (48c)$$

The derivative $\frac{\partial \varepsilon_{pq}}{\partial C_{kv}^E}$ in (47) can use the first Padé approximation (48c) as the final $\mathbf{C}^E$ is employed, which for metal plasticity is sufficiently close to the unitary matrix Brunig (1999); Baaser (2004). In this case:

$$\frac{\partial \varepsilon_{pq}}{\partial C_{kv}^E} \cong \frac{\partial \varepsilon_{pq}^0}{\partial C_{kv}^E} = (\delta_{pk} - \varepsilon_{pk}^0)(\mathbf{I} + \mathbf{C}^E)_{vq}^{-1}$$

In our present application, we employ J_2 associative plasticity, where the dissipation potential $\mathcal{F}$ coincides with the yield function (see also Areias, César de Sá, and António (2003)).

5.2 Cohesive model

The virtual work of the cohesive forces is included in the term δW_E. The force introduced by this term corresponds
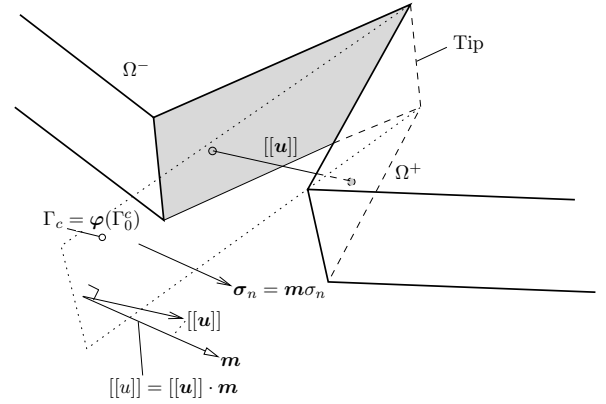

Figure 3 : Cohesive forces arising from the crack surface separation.

to the resistance to opening, which is a function of the opening displacement itself. Because this type of dissipation mechanism occurs on a set of measure zero, part of the energy dissipated in the continuum is transferred to the cohesive law. The opening displacement can be written as a function of the mid-surface position on both sides of the crack *and* the director on both sides of the crack. We denote the surface opening by $[[u]]$, which can be expressed as (see figure 3):

$$[[u]] = [[\boldsymbol{u}]] \cdot \boldsymbol{m} \quad (49)$$

where $[[\boldsymbol{u}]]$ is defined according to:

$$[[\boldsymbol{u}]] = [[\boldsymbol{r}]] + \theta^3 [[\boldsymbol{n}]] \quad (50)$$

where $[[\boldsymbol{r}]]$ is the mid-surface displacement jump and $[[\boldsymbol{n}]]$ is the director field jump. These are evaluated at the crack surface $\boldsymbol{X} \in \Gamma_0^c$.

If we denote the part of δW_E corresponding to the cohesive virtual work as δW_E^c, then we can write it using the Kirchhoff stress value σ_n as:

$$\delta W_E^c = -\int_{\Gamma_O^c} \sigma_n \delta[[u]] \mathrm{d}A = -\int_{\Gamma_O^c} \boldsymbol{\sigma_n} \cdot \delta[[\boldsymbol{u}]] \mathrm{d}A \quad (51)$$

where A represents the area of Γ_0^c.

The first variation of δW_E^c is required for the application of the Newton method. It can be written as:

$$\mathrm{d}\delta W_E^c = -\int_{\Gamma_O^c} \mathrm{d}[[\boldsymbol{u}^T]] \boldsymbol{K} \delta[[\boldsymbol{u}]] \mathrm{d}A \quad (52)$$

with

$$K = \frac{\partial \sigma_n}{\partial [[u]]} \boldsymbol{m} \otimes \boldsymbol{m} \qquad (53)$$

We use the particular constitutive model for the cohesive zone given by:

$$\sigma_n = \frac{\sigma_{max}}{\epsilon} \exp \left(-\frac{\sigma_{max}}{G_f} \epsilon \right) [[u]] \qquad (54)$$

where σ_{max} is the maximum cohesive stress, G_f is the fracture (surface) energy and $\epsilon = \max_{history} [[u]]$ denotes an internal variable. A penalty term is employed to attenuate crack face inter-penetration.

6 Examples

6.1 Linear elastic shell

Consider a linear shell problem as shown in figure 4. This example is studied to investigate membrane locking. Note that we don't exploit symmetry but model the entire cylinder. The shell consists of a pinched cylinder with rigid end diaphragms and has been analyzed by e.g. Simo, Fox, and Rifai (1989); Parish (1991); Bucalem and Bathe (1993); Hauptmann and Schweizerhof (1998). The displacement at the load position is of interest. The results for the 4 node selectively integrated quadrilateral (SRI) are taken from Belytschko and Wong (1989). A value of 1.82488×10^{-5} (c.f. Kasper and Taylor (2000)) consistent units is adopted as a reference. We tested second and third order complete shape functions. Second order complete shape functions will have additional 6 nodal parameters to the usual 3 nodal parameters, while third order complete shape functions have additional 9 nodal parameters.

The results are shown in figure 5 in terms of the normalized displacements. Since we compare the results to results obtained with (quadrilateral) finite elements, the nodes are arranged such that they span one background cell that is used for integration. The number of background cells will correspond to the number of finite elements and the number of nodes are equivalent in the meshfree and FE simulations. As can be seen, second order complete MLS leads to much stiffer results that indicates locking. An approach with third order completeness gives much better results. Our method performs
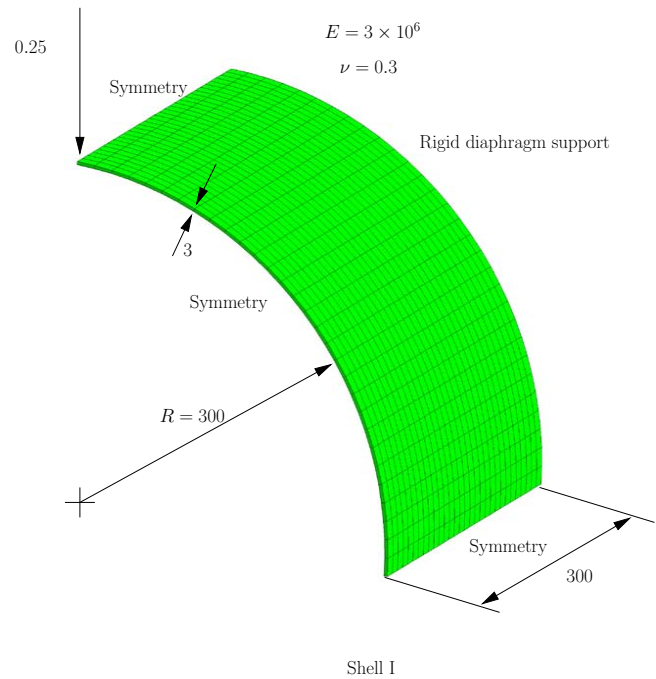

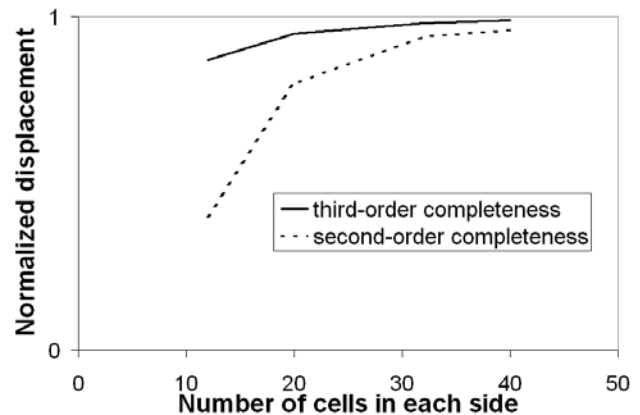**Figure 4** : Set-up of the linear pinched clamped cylinder

Figure 5 : Load-displacement curve of the linear pinched clamped cylinder for different orders of completeness

well compared to several results obtained with finite elements, see figure 6.

6.2 Static hemi-spherical punch

Lee, Woertz, and Wierzbicki (2004) carried out experimental, analytical and numerical studies on rectangular thin plates subjected to a hemi-spherical punch. The test-setup is shown in figure 7. They modified the relation
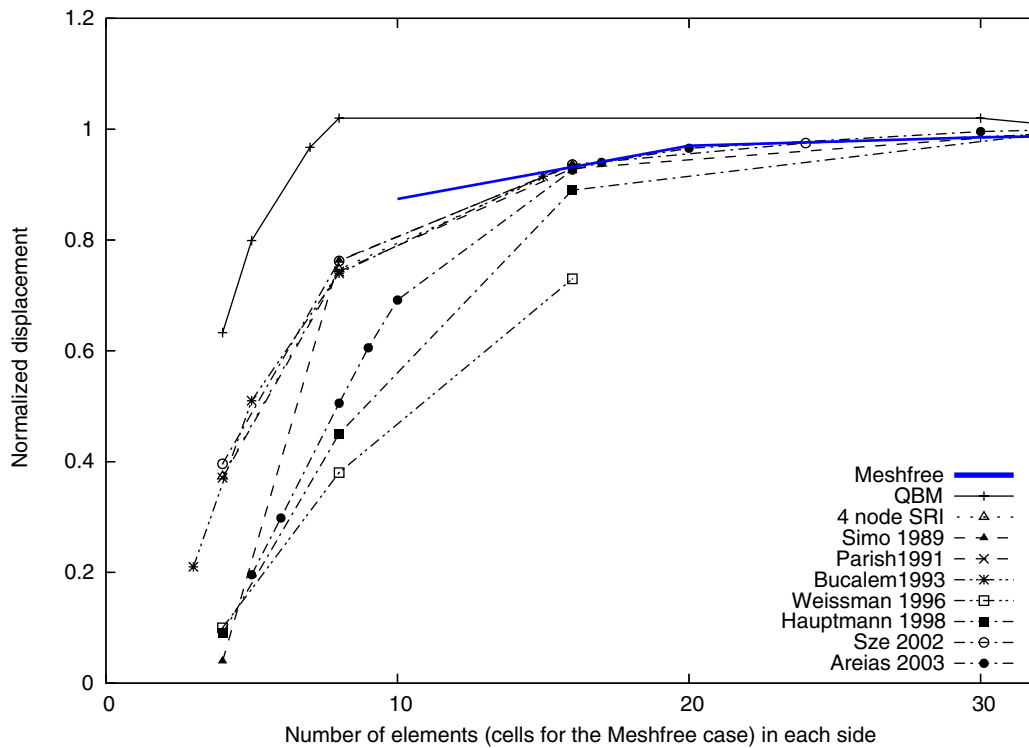
Figure 6 : Load-displacement curve of the linear pinched clamped cylinder with other methods
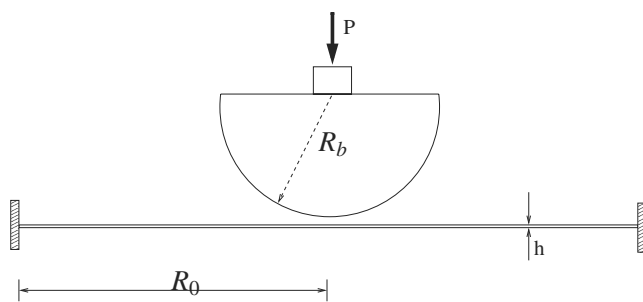

Figure 7 : Test-setup of the hemi-spherical punch problem of Lee, Woertz, and Wierzbicki (2004)

$\xi = R_b/R_0$ where R_b is the diameter of the sphere and R_0 is the half length of the plate as shown in figure 7. They also studied different plate thickness. We will present results for two examples, for parameters $R_b = 75$mm, $R_0 = 110$mm and plate thickness $h_0 = 1.4$mm and $R_b = 50$mm, $R_0 = 110$mm and $h_0 = 1.14$mm. We used J_2 plasticity and adopted the power hardening law from Lee, Woertz, and Wierzbicki (2004) $\sigma = C_0 \varepsilon^n$ with $C_0 = 586$MPa and $n = 0.22$. Fracture is introduced when the effective plastic

strains exceed a value of 0.45. As shown e.g by McClintock (1968); Bao and Wierzbicki (2004), damage evolution in ductile fracture depends on the stress triaxiality. Since the stress triaxiality is nearly constant in this example, the effective strain is sufficient for crack initiation. The fracture energy for the cohesive law is $G_f = 100N/m$ with exponential decay as described in section 5.2.

We discretized the plate with different numbers of particles (49,000 particles and 12,000 particles). In addition we carried out an adaptive computation starting from 3,000 particles. The adaptive approach is based on the estimation of the approximation error, meaning particles are added where high strain gradients occur. A detailed description can be found in Rabczuk and Belytschko (2005).

For the plate with $R_b = 75$mm, $R_0 = 110$mm, $h_0 = 1.4$mm, the deformation of the plate at different times for the 49,000 particle discretization is shown in figure 8a,b,d,f. The crack pattern agrees well with the experimental and numerical crack pattern from Lee, Woertz, and Wierzbicki (2004). Also the fracture radius of approximately 51cm is reproduce correctly by our simulation. Note that Lee, Woertz, and Wierzbicki (2004) al-
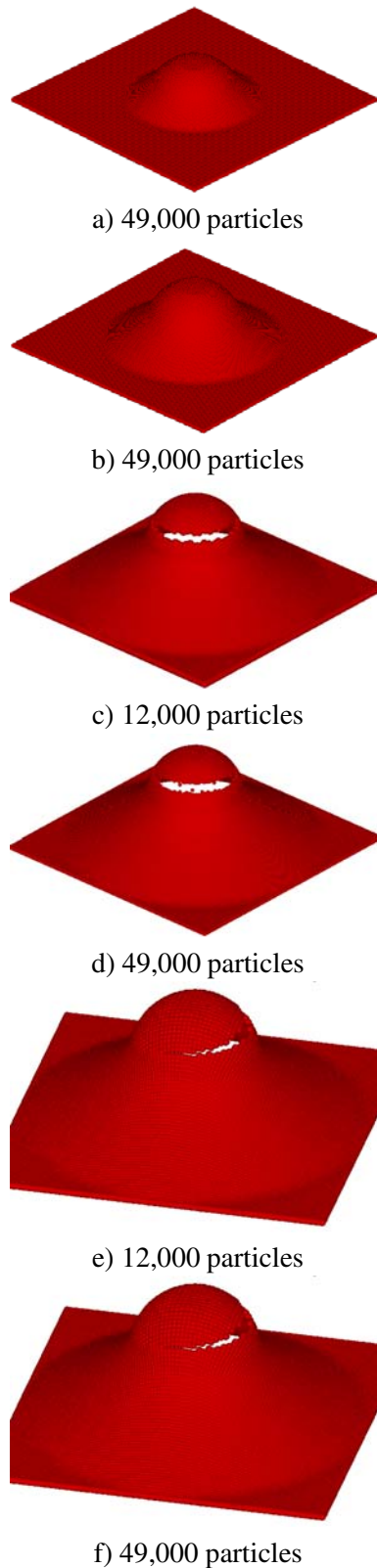
a) 49,000 particles

b) 49,000 particles

c) 12,000 particles

d) 49,000 particles

e) 12,000 particles

f) 49,000 particles

Figure 8 : Deformation of the shell of the hemispherical punch problem ($R_b = 75$mm, $R_0 = 110$mm, $h_0 = 1.4$mm) at different load steps, with two different refinements and at different view points
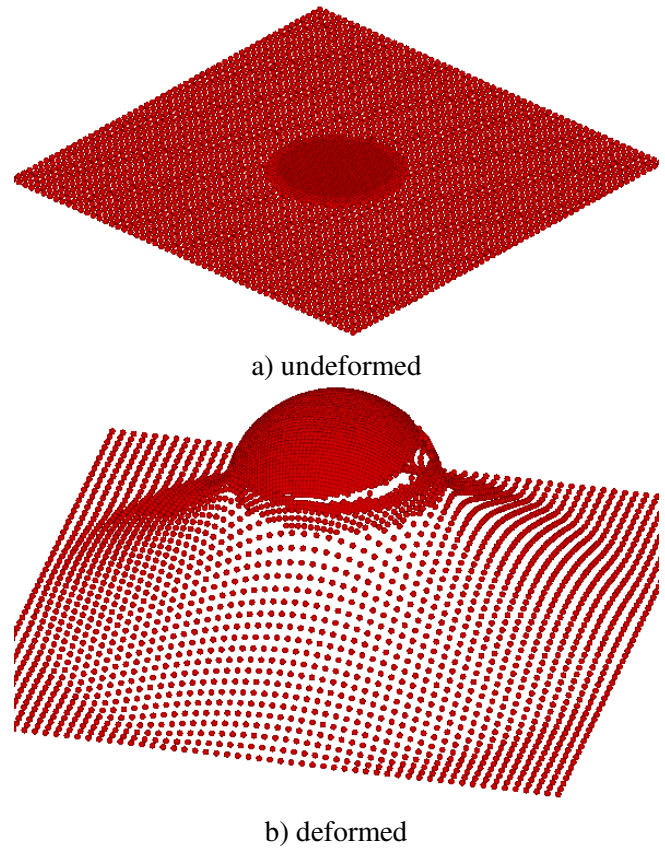

a) undeformed

b) deformed

Figure 9 : Shell of the hemispherical punch problem ($R_b = 75$mm, $R_0 = 110$mm, $h_0 = 1.4$mm) at the end of the adaptive computation, a) projection in the undeformed configuration, b) deformed configuration

ligned the mesh according to the crack pattern, i.e. they arranged the elements in circles, whereas we obtained a curved crack pattern with a structured particle discretization.

The final crack pattern for the three different simulations is shown in figure 8e,f and 9b and looks almost identical. In the adaptive simulation, we allowed two refinement steps. The "projected" refinement into the initial configuration at the end of the computation is shown in figure 9a. We would like to note that in the experiment the crack does not encompass the entire circumference. This is reproduced well by the numerical simulation though we expected a uniform separation of the cap from the plate.

We have run the same example also with the method proposed in Rabczuk, Areias, and Belytschko (submitted) that employs an intrinsic basis. The results look almost
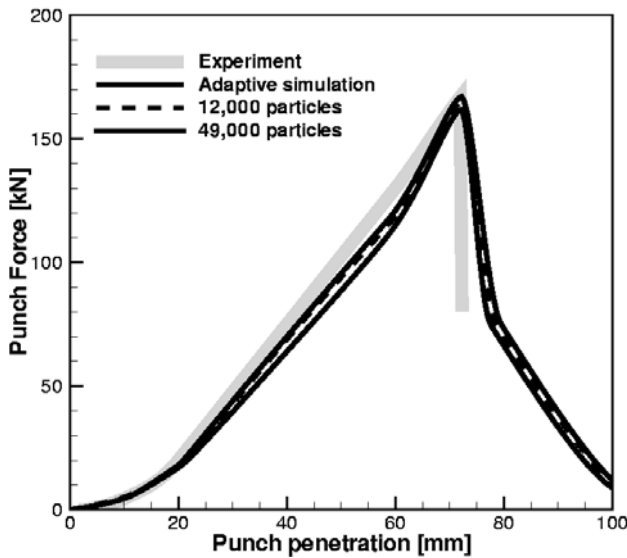
a)
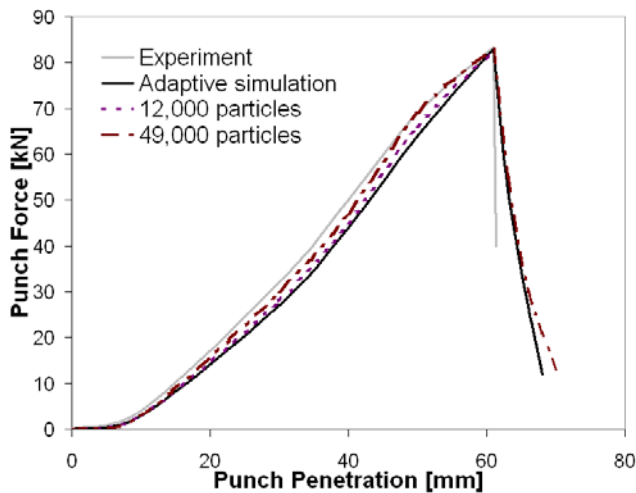
b)

Figure 10 : Load-displacement curve of the hemispherical punch problem of Lee, Woertz, and Wierzbicki (2004) for the following parameters:a) $R_b = 75$mm, $R_0 = 110$mm and $h_0 = 1.4$mm, b) $R_b = 50$mm, $R_0 = 110$mm and $h_0 = 1.14$mm

identical and therefore are not presented here. However, our new method is between two to three times faster than our recent method. In the recent method, at least 121 neighboring particles in the domain of influence are necessary while it is here sufficient to include only 21 neighboring paticles in the domain of influence. The adaptive computation decreases the computation time about another factor of three.

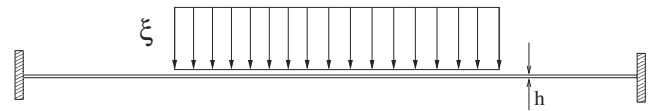The load deflection curve for the different simulations

Figure 11 : Test-setup of the plate under impulsive loading of Lee and Wierzbicki (2005a,b)

compared to the experimental results is shown in figure 10a. The load-displacement curve for the other parameters set ($R_b = 50$mm, $R_0 = 110$mm and $h_0 = 0.9$mm) is shown in figure 10b. The agreement is excellent and no mesh dependence occurs.

6.3 Thin plates under localized impulsive loading

Lee and Wierzbicki (2005a,b) performed experimental and numerical/analytical studies on circular thin plates subjected to impulsive and impact loading. A typical test setup is shown in figure 11. The impulsive loading is simplified modelled as applied impulse, i.e. as pressure time history or velocity initial condition. They found three different failure mechanisms. For low impulses, dishing occurs, i.e. the plate undergoes large inelastic deformation without failure. The second phase is discing that is characterized by circumferential cracking. The third and last phase is petalling where radial cracks propagate after the *cap* has fractured.

We will study the same examples as in Lee and Wierzbicki (2005b). The geometric data is radius $R_0 = 5416$mm and plate thickness $h_0 = 16$mm. A circular load of radius R_L is applied. Two different load radii are investigated with $\xi_0 = R_L/R_0$ with $\xi_0 = 0.25$ and $\xi_0 = 0.5$. The non-dimensional impulse $V = I_0 (c\rho h)$ with sound speed c, density ρ and impulse $I_0 = p_0 t_0$ where p_0 is the pressure peak and t_0 is the relaxation time, is varied as well. The different values for V are 0.92, 1.24, 1.45 and 2.42 for the $\xi = 0.25$-plate and 0.92, 1.24 and 1.45 for the $\xi = 0.5$-plate.

We used J_2 plasticity with power law $\sigma = 1018\varepsilon^{0.17}$. The effective plastic strain to fracture is 0.3. The fracture energy for the exponential cohesive law is $G_f = 100N/m$.

We used again a structured particle arrangement. The discretization was produced by a procedure explained in Rabczuk and Belytschko (2005). We tested two different particle discretizations, 10,000 particles and 40,000 particles. Exemplarily for the computation with $\xi = 0.25$
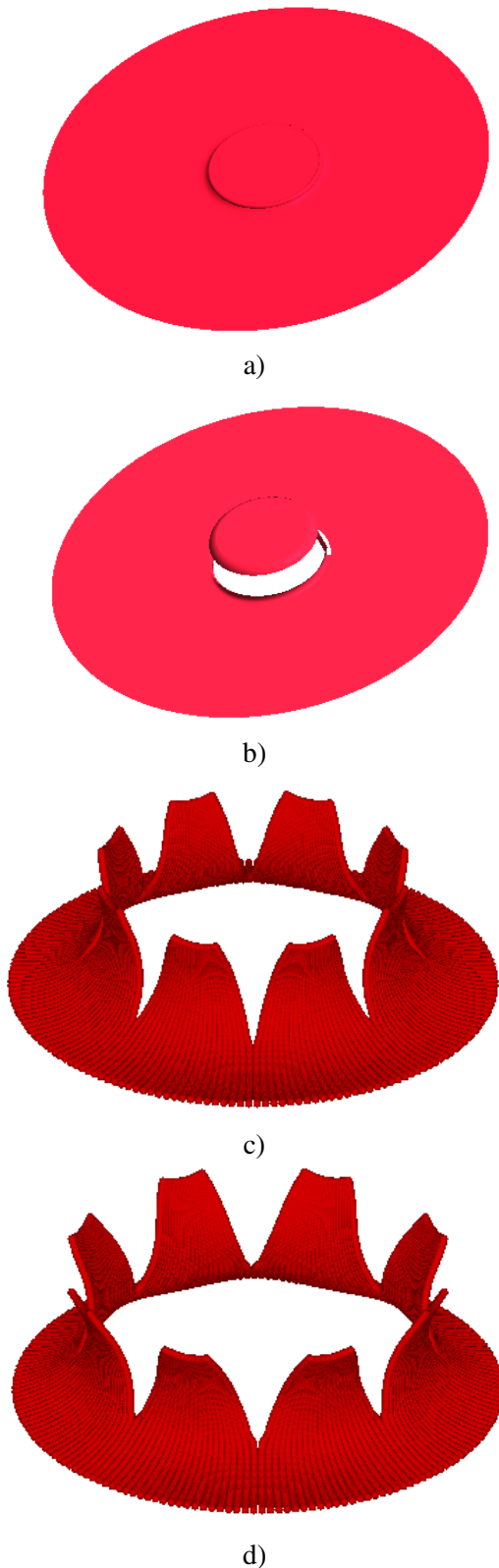
a)

b)

c)

d)

Figure 12 : Petalling of the Lee and Wierzbicki (2005b) plate at different time step, $\xi = 0.25$, $V = 2.42$
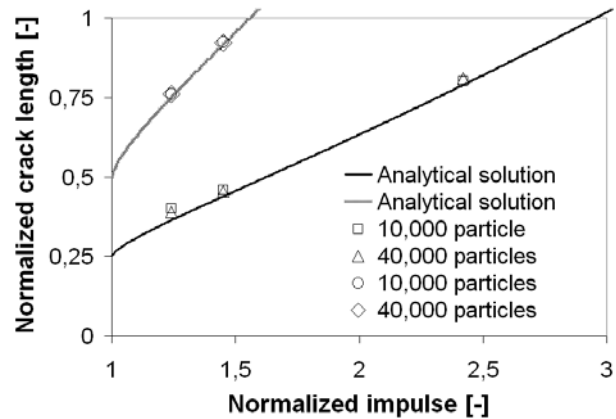

Figure 13 : Normalized crack length-normalized impulse curve for different impulses and ξ_0, the numerical results are compared to the analytical solution of Lee and Wierzbicki (2005a,b)

and $V = 3$, deformations at different times of the 40,000 particle computation are shown in figure 12. The results agree well with the experimental and analytical results in Lee and Wierzbicki (2005b).

The normalized crack length-normalized impulse curves for the different cases are shown in figure 13 and compared with the analytical predictions according to Lee and Wierzbicki (2005b). They are in good agreement. At a normalized impulse of approximately 0.92, the normalized cracks length is zero-as in the analytical prediction-and therefore not included in the figure.

7 Conclusions

We have presented a meshfree thin shell formulation based on an extrinsic enrichment for arbitrary evolving cracks. Cracks are represented by cohesive segments that are located at the particle position. The representation of the crack as set of cracked particles instead of continuous line facilitates the implementation and application to multiple cracking and crack branching as shown for petalling of a plate under explosive loading. In this example, several radial cracks as well as circumferential cracks occured. Crack initiation and propagation happened quite natural in this method. The crack is introduced over the entire thickness. Regarding the thickness of the shell, this assumption seems to be reasonable.

Third order completeness was necessary to remove mem-

brane locking. This was achieved by an extrinsic basis, i.e. by adding additional degrees of freedom. We have chosen zero-order complete Shepard functions, so to obtain third order completeness, 9 additional unknowns per node have to be introduced, not considering the enrichment for cracked particles. This seemed to be a lot. However, in comparison to the method in Rabczuk, Areias, and Belytschko (submitted), where a similar meshfree shell was proposed with intrinsic enrichment, the computational cost here is at least 2 times lower. This is due to the fact that a much smaller domain of influence can be used as in Rabczuk, Areias, and Belytschko (submitted). We also tested the extrinsic enrichment versus intrinsic MLS enrichment with respect to computational cost. Since only a few nodes are enriched, the influence of the enrichment strategy with respect to computational cost is low.

We tested the method for several cracking problems and compared the results to experimental data, analytical solutions and other numerical results from the literature. The results agreed very well. Probably the most tricky part is the surface parametrization of the method. To be able to discretize more complex geometries such as folded plates or honeycomb structures, the surface has to be subdivided into surfaces that are connected to each other by e.g. Lagrange multipliers. This is still topic of ongoing investigations.

References

Areias, P.; César de Sá, J.; António, C. (2003): A gradient model for finite strain elastoplasticity coupled with damage. *Finite Elements in Analysis and Design*, vol. 39, pp. 1191–1235.

Areias, P.; Song, J.; Belytschko, T. (): Analysis of fracture in thin shells by overlapping paired elements. *in progress*.

Areias, P.; Song, J.; Belytschko, T. (2005): A simple finite-strain quadrilateral shell element part i: Elasticity. *International Journal for Numerical Methods in Engineering*, vol. in press.

Atluri, S. (1984): Alternate stress and conjugate strain measures, and mixed variational formulations involving rigid rotations, for computational analysis of finitely deformed plates and shells: Part i: Theory. *Computers and Structures*.

Atluri, S. (2002): *The Meshless Local Petrov-Galerkin (MLPG) Method*. Tech Science Press.

Atluri, S.; Cazzani, A. (1994): Rotations in computational solid mechanics. *Archives in Computational Mehtods in Engineering, ICNME, Barcelona, Spain*.

Atluri, S.; Shen, S. (2002): The meshless local petrov-galerkin (mlpg) method: a simple and less-costly alternative to the finite element and boundary element methods. *CMES: Computer Modeling in Engineering & Sciences*, vol. 3, pp. 11–51.

Atluri, S.; Zhu, T. (1998): A new meshless local petrov-galerkin (mlpg) approach in computational mechanics. *Computational Mechanics*, vol. 22, pp. 117–127.

Atluri, S.; Zhu, T. (2000): The meshless local petrov-galerkin (mlpg) approach for solving problems in elastostatics. *Computational Mechanics*, vol. 25, pp. 169–179.

Baaser, H. (2004): The Padé-approximation for matrix exponentials applied to an integration algorithm preserving plastic incompressibility. *Computational Mechanics*, vol. 34, pp. 237–245.

Bao, Y.; Wierzbicki, T. (2004): On fracture locus in the equivalent strain an stress triaxiality space. *International Journal of Mechanical Sciences*.

Batoz, J.; Hammadi, F.; Zheng, C.; Zhong, W. (2000): On the linear analysis of plates and shells using a new-16 degrees of freedom flat shell element. *Computers and Structures*, vol. 78, pp. 11–20.

Batoz, J.; Zheng, C.; Hammadi, F. (2001): Formulation and evaluation of new triangular, quadrilateral, pentagonal and hexagonal discrete kirchhoff plate/shell elements. *International Journal for Numerical Methods in Engineering*, vol. 52, pp. 615–630.

Belytschko, T.; Liu, W. K.; Moran, B. (2000): *Nonlinear Finite Elements for Continua and Structures*. John Wiley and Sons, Chichester.

Belytschko, T.; Lu, Y. (1995): Element-free galerkin methods for static and dynamic fracture. *International Journal of Solids and Structures*, vol. 32, pp. 2547–2570.

Belytschko, T.; Lu, Y.; Gu, L. (1994): Element-free galerkin methods. *International Journal for Numerical Methods in Engineering*, vol. 37, pp. 229–256.

Belytschko, T.; Wong, B. (1989): Assumed strain stabilization procedure for the 9−node Lagrange shell element. *International Journal for Numerical Methods in Engineering*, vol. 28, pp. 385–414.

Brunig, M. (1999): Large strain elasto-plastic theory and nonlinear finite element analysis based on metric transformation tensors. *Computational Mechanics*, vol. 24, pp. 187–196.

Bucalem, M.; Bathe, K.-J. (1993): Higher-order MITC general shell elements. *International Journal for Numerical Methods in Engineering*, vol. 36, pp. 3729–3754.

Chen, J.; Wang, D.; Dong, S. (2004): An extended meshfree method for boundary value problems. *Computer Methods in Applied Mechanics and Engineering*, vol. 193, no. 12-14, pp. 1085–1103.

Crisfield, M.; Tan, D. (2001): Large-strain elasto-plastic shell analysis using low-order elements. *Engineering Computations*, vol. 18, pp. 255–285.

Crisfield, M.; Tan, D. (2001): Rotation shape functions for a low-order quadrilateral plate element with mid-side rotations. *Communications in numerical methods in engineering*, vol. 17, pp. 191–199.

Dawe, D. (1972): Shell analysis using a simple facet element. *Journal of Strain Analysis*, vol. 7, no. 4, pp. 266–270.

D.D., W.; Chen, J. (2004): Locking-free stabilized conforming nodal integration for meshfree mindlin-reissner plate formulation. *Computer Methods in Applied Mechanics and Engineering*, vol. 193, no. 12-14, pp. 1065–1083.

Duarte, C.; Oden, J. (1996): An h-p adaptive method using clouds. *Computer Methods in Applied Mechanics and Engineering*.

Duarte, C.; Oden, J. (1996): H-p clouds- an h-p meshless method. *Numer. Methods Partial Differential Equations*.

Fraeijs de Veubeke, B. (1968): A conforming finite element for plate bending. *International Journal of Solids and Structures*, vol. 4, pp. 95–108.

Garcia, O.; Fancello, E.; de Barcellos, C.; Duarte, C. (2000): hp-clouds in mindlin's thick plate model. *International Journal for Numerical Methods in Engineering*, vol. 47, no. 8, pp. 1381–1400.

Han, W.; Reddy, B. (1999): *Plasticity. Mathematical theory and numerical analysis*, volume 9 of *Interdisciplinary Applied Mathematics*. Springer.

Hauptmann, R.; Schweizerhof, K. (1998): A systematic development of solid-shell element formulations for linear and non-linear analyzes employing only displacement degrees of freedom. *International Journal for Numerical Methods in Engineering*, vol. 42, pp. 49–69.

Herrmann, L. (1967): Finite-element analysis for plates. *ASCE Journal of the Engineering Mechanics Division*, vol. 93, no. EM-5, pp. 13–26.

Irons, B. (1976): The semiloof shell element. *Finite elements for thin shells and curved members*, pp. 197–222. Wiley, New York, 1976.

Kasper, E.; Taylor, R. (2000): A mixed enhanced strain method: Part i: geometrically linear problems. *Computers and Structures*, vol. 75, pp. 237–250.

Kim, N.; Choi, K.; Chen, J.; Botkin, M. (2002): Meshfree analysis and design sensitivity analysis for shell structures. *International Journal for Numerical Methods in Engineering*, vol. 53, no. 9, pp. 2087–2116.

Kolahi, A.; Crisfield, M. (2001): A large-strain elasto-plastic shell formulation using the Morley triangle. *International Journal for Numerical Methods in Engineering*, vol. 52, pp. 829–849.

Krysl, P.; Belytschko, T. (1996): Analysis of thin shells by the element-free galerkin method. *International Journal of Solids and Structures*, vol. 33, no. 20-22, pp. 3057–3078.

Lee, E. (1969): Elasto-plastic deformation at finite strains. *ASME Journal of Applied Mechanics*, vol. 36, pp. 1–6.

Lee, Y.; Wierzbicki, T. (2005): Fracture prediction of thin plates under localized impulsive loading. part i: dishing. *International Journal of Impact Engineering*.

Lee, Y.; Wierzbicki, T. (2005): Fracture prediction of thin plates under localized impulsive loading. part ii:

discing and petalling. *International Journal of Impact Engineering*.

Lee, Y.; Woertz, J.; Wierzbicki, T. (2004): Fracture prediction of thin plates under hemi-spherical punch with calibration and experimental verification. *International Journal of Mechanical Sciences*.

Li, Q.; Soric, J.; Jarak, T.; Atluri, S. (2005): A locking-free meshless local petrov-galerkin formulation for thick and thin plates. *Journal of Computational Physics*.

Li, S.; Hao, W.; Liu, W. (2000): Numerical simulations of large deformation of thin shell structures using meshfree methods. *Computational Mechanics*, vol. 25, no. 2-3, pp. 102–116.

Maugin, G. (1994): Eshelby stress in elastoplasticity and ductile fracture. *International Journal of Plasticity*.

McClintock, F. (1968): A criterion of ductile fracture by growth of voids. *Journal of Applied Mechanics*.

Melenk, J. M.; Babuska, I. (1996): The partition of unity finite element method: Basic theory and applications. *Computer Methods in Applied Mechanics and Engineering*, vol. 139, pp. 289–314.

Miehe, C. (1998): A constitutive frame of elastoplasticity at large strains based on the notion of a plastic metric. *International Journal of Solids and Structures*, vol. 35, no. 30, pp. 3859–3897.

Nagtegaal, J.; Slater, J. (1981): A simple non-compatible thin shell element based on discrete kirchhoff theory. *Nonlinear finite element analysis of plates and shells, ASME, AMD*, vol. 48, pp. 167–192.

Noguchi, H.; Kawashima, T.; Miyamura, T. (2000): Element free analysis of shell and spatial structures. *International Journal for Numerical Methods in Engineering*, vol. 47, no. 6, pp. 1215–1240.

Parish, H. (1991): An investigation of a finite rotation four node assumed strain shell element. *International Journal for Numerical Methods in Engineering*, vol. 31, pp. 127–150.

Peng, D. P.; Merriman, B.; Osher, S. (1999): A pde-based fast local level set method. *Journal of Computational Physics*, vol. 155, pp. 410–438.

Rabczuk, T.; Areias, P.; Belytschko, T. (submitted): A meshfree thing shell for large deformation, finite strain and arbitrary evolving cracks. *International Journal for Numerical Methods in Engineering*.

Rabczuk, T.; Belytschko, T. (2004): Cracking particles: A simplified meshfree method for arbitrary evolving cracks. *International Journal for Numerical Methods in Engineering*, vol. 61, no. 13, pp. 2316–2343.

Rabczuk, T.; Belytschko, T. (2005): Adaptivity for structured meshfree particle methods in 2D and 3D. *International Journal for Numerical Methods in Engineering*, vol. 63, no. 11, pp. 1559–1582.

Rabczuk, T.; Belytschko, T. (2006): Application of meshfree particle methods to static fracture of reinforced concrete structures. *International Journal of Fracture*, vol. 137, no. 1-4, pp. 19–49.

Simo, J.; Fox, D.; Rifai, M. (1989): On a stress resultant geometrically exact shell model. Part II: The linear theory; computational aspects. *Computer Methods in Applied Mechanics and Engineering*, vol. 73, pp. 53–92.

Song, J.-H.; Areias, P.; Belytschko, T. (2006): A method for dynamic crack and shear band propagation with phantom nodes. *International Journal for Numerical Methods in Engineering*.

Strouboulis, T.; Copps, K.; Babuška, I. (2000): The generalized finite element method: An example of its implementation and illustration of its performance. *International Journal for Numerical Methods in Engineering*, vol. 47, no. 8, pp. 1401–1417.